



Magnetic properties of heat treated bacterial ferrihydrite nanoparticles



D.A. Balaev^{a,b}, A.A. Krasikov^{a,b,*}, A.A. Dubrovskiy^{a,d}, S.I. Popkov^{a,b}, S.V. Stolyar^{a,b},
O.A. Bayukov^a, R.S. Iskhakov^a, V.P. Ladygina^c, R.N. Yaroslavtsev^b

^a Kirensky Institute of Physics, Russian Academy of Sciences, Siberian Branch, Krasnoyarsk 660036, Russia

^b Siberian Federal University, Krasnoyarsk 660041, Russia

^c Presidium of Krasnoyarsk Scientific Center, Russian Academy of Sciences, Siberian Branch, Krasnoyarsk 660036, Russia

^d International Laboratory of High Magnetic Fields and Low Temperatures, Gajowicka 95, 53-421 Wroclaw, Poland

ARTICLE INFO

Article history:

Received 30 April 2015

Received in revised form

8 February 2016

Accepted 19 February 2016

Available online 20 February 2016

Keywords:

Ferrihydrite

Nanoparticles

Superparamagnetism

ABSTRACT

The magnetic properties of ferrihydrite nanoparticles, which are products of vital functions of *Klebsiella oxitoca* bacteria, have been studied. The initial powder containing the nanoparticles in an organic shell was subjected to low-temperature ($T=160\text{ }^{\circ}\text{C}$) heat treatment for up to 240 h. The bacterial ferrihydrite particles exhibit a superparamagnetic behavior. Their characteristic blocking temperature increases from 26 to 80 K with the heat treatment. Analysis of the magnetization curves with regard to the magnetic moment distribution function and antiferromagnetic contribution shows that the low-temperature heat treatment enhances the average magnetic moment of a particle; i.e., the nanoparticles coarsen, probably due to their partial agglomeration during heat treatment. It was established that the blocking temperature nonlinearly depends on the particle volume. Therefore, a model was proposed that takes into account both the bulk and surface magnetic anisotropy. Using this model, the bulk and surface magnetic anisotropy constants $K_V \approx 1.7 \times 10^5 \text{ erg/cm}^3$ and $K_S \approx 0.055 \text{ erg/cm}^2$ have been determined. The effect of the surface magnetic anisotropy of ferrihydrite nanoparticles on the observed magnetic hysteresis loops is discussed.

© 2016 Elsevier B.V. All rights reserved.

1. Introduction

It is well-known that the magnetic properties of anti-ferromagnetic (AF) particles fundamentally change at the nanoscale [1–7]; specifically, the AF susceptibility increases and its temperature dependence is modified [2,3,6,8,9]. As a rule, the spin-flop transition field [10,11] and the magnetic ordering (Néel) temperature decrease [6,12–15] (the exception found in MnO where surface oxidation puts the MnO core under strain, leading to a decrease of cell parameters and increase of exchange interaction [4,16]). In addition, if a spin system undergoes the magnetic transition, the latter shifts toward lower temperatures (e.g., the Morin point in hematite [1,7,10,11]). Finally, the magnetization curve $M(H)$ drastically changes due to the occurrence of an uncompensated magnetic moment in small AF particles [3,6–9,14], which causes a superparamagnetic (SP) behavior of such a system. Obviously, these properties are mainly due to the surface effects, which start playing a key role as the particle size is decreased. Moreover, the presence of defects both on the surface and in the bulk of nanoparticles becomes extremely important.

Possible reasons for the occurrence of the uncompensated magnetic moment in an AF nanoparticle were formulated by Néel [17]. These can be either random AF order breaks, i.e., partial decompensation of spins of magnetically active atoms due to the presence of defects on the surface or in the bulk of a particle, or an odd number of planes with parallel spins. Uncompensated magnetic moment μ_{un} of a particle depends on number N of magnetically active atoms with magnetic moment μ :

$$\mu_{\text{un}} \approx \mu \cdot N^b. \quad (1)$$

If, from the statistical considerations, the number of defects is proportional to N^b , then exponent b amounts to 1/3 and 1/2 for the cases of surface and bulk defects, respectively, and to 2/3 for the case of the odd number of planes with parallel spins. When $N \sim 10^4$ and smaller, the μ_{un} value is not vanishingly small any more and is comparable with the magnetic moment of ferri- or ferromagnetic nanoparticles [7,18], in which surface atoms often do not participate in the formation of the magnetic moment and form the so-called magnetically dead layer [19–22]. Therefore, AF nanoparticles can compete with ferro- and ferrimagnetic nanoparticles in various applications, including targeted drug delivery inside the human body [23–25]. This circumstance, along with still unexplained features of the magnetic properties, stimulates the intensive studies of AF nanoparticles [1–16,26,27–32]. Among

* Corresponding author at: Kirensky Institute of Physics, Russian Academy of Sciences, Siberian Branch, Krasnoyarsk 660036, Russia

various AF materials, biogenic particles, including ferritin ones [33–40], evoke special interest. Ferritin contained in almost all living organisms works as an iron store, comprising up to 30% of iron atoms in the organism. Ferritin particles form an AF ordered iron hydroxide matrix inside a protein shell with outer and inner diameters of 12 and 5–8 nm, respectively. Horse spleen ferritin is currently a commercial product. Studies of the magnetic properties of horse spleen ferritin showed that this material exhibits the SP behavior with the characteristic blocking temperature $T_B \approx 12$ K and the extraordinary temperature behavior of μ_{un} and AF susceptibility [34–44].

Ferrihydrite with the nominal formula $5Fe_2O_3 \cdot 9H_2O$ (the water content can be different), is an iron hydroxide version. This mineral is widely spread in aqueous systems on the Earth's surface. Ferrihydrite nanoparticles can form during the vital activity of living organisms, e.g., bacteria.

It was established [45–47] that *Klebsiella oxytoca* bacteria produce ferrihydrite nanoparticles. Further investigations of the obtained biogenic material showed that it exhibits the SP behavior [48]. Additional purification of the biogenic sediments allowed obtaining a powder consisting of ferrihydrite nanoparticles, which repeatedly demonstrated the existence of a blocking temperature of about 20 K [49]. It was found that heat treatment of this powder in air for 3 h at temperatures slightly higher than the boiling point of water (140–160 °C) leads to the variation in the magnetic properties, specifically, doubles the blocking temperature [50]. Analysis of the magnetization curves [50] showed that during annealing the particles coarsen. In this study, we investigated a powder from nanoparticles produced by *Klebsiella oxytoca* bacteria from the other set (the blocking temperatures of initial nanoparticles from the two parties differ by about 3 K), which were subjected to heat treatment at a temperature of 160 °C for much longer time (up to 240 h). At such a relatively low temperature, we may assume that ferrihydrite, on which the nanoparticles based, does not undergo the transition to the other iron oxide phases, in contrast to the case of annealing at 500 °C [51], while the water (or, to be exact, the OH group) content in it can decrease. The aim of this work was to study modification of the magnetic properties of bacterial ferrihydrite subjected to the heat treatment under these conditions.

2. Experimental

2.1. Sample preparation and HRTEM studies

The *Klebsiella oxytoca* strain used in this work was separated from the sapropel of the Borovoe lake, Krasnoyarsk region. Microorganisms were inoculated into an agar medium and grown under anaerobic conditions. After multiple ultrasonic processing of bacterial sediments, centrifugation, and washing, a stable sol of nanoparticles in an aqueous solution was fabricated and was then dried. The obtained powder of magnetic nanoparticles is hereinafter referred to as 0 h. A part of the powder was kept in air at a temperature of 160 °C for different times of up to 240 h in a drying oven. The initial and annealed powders were objects of study. Hereinafter, the prepared samples are referred to as 0 h, 3 h, 8 h, 24 h, and 240 h in accordance with their annealing time.

It was found that during heat treatment the powder loses its mass, which can be attributed to the intercrystalline water (OH group) loss. The mass loss for samples 3 h, 8 h, 24 h, and 240 h was about 18%, 20%, 22%, and 26%, respectively. After keeping the annealed powder in air and in a saturated water vapor at room temperature, the sample mass increases yet remains smaller than its initial value.

Transmission Electron Microscopy (TEM) studies were performed with Hitachi HT7700 facility. The powder diluted in

alcohol was subjected to the ultrasonic bath followed by coating on the support mesh grid.

2.2. Magnetic and Mössbauer studies

The samples were characterized and the iron state was established using the Mössbauer technique. Powder samples with a mass thickness of 5–10 mg/cm² were investigated on an MC-1104Em Mössbauer spectrometer with a ⁵⁷Co(Cr) source using the natural iron content. Chemical shifts were measured relative to α -Fe.

Temperature and field dependences of the magnetic moment $M(T)$ и $M(H)$ were determined on a vibrating sample magnetometer [52]. The powder under study was fixed in a measuring capsule in paraffin. The magnetic measurement data were corrected using the diamagnetic signal from the capsule with paraffin. The $M(T)$ dependences were obtained in the zero-field cooling (ZFC) and field cooling (FC) regimes. The hysteresis loops $M(H)$ at $T=4.2$ K were measured in the ZFC regime.

3. Results and discussion

3.1. Mössbauer study and TEM micrographs

X-ray diffraction patterns of the powders obtained using the technique described above are typical of the amorphous state [51]. Therefore, we used Mössbauer spectroscopy to identify the crystal-chemical structure and obtain information on possible variations in the local environment of iron and the occurrence of other iron oxide phases during heat treatment.

Fig. 1a shows room-temperature Mössbauer spectra of the investigated samples. The spectra are quadrupole doublets with different line broadenings. Analysis of the quadrupole splitting distribution $P(QS)$ in the experimental spectra (Fig. 1b) shows the presence of several nonequivalent iron positions with different distortions of the local environment. The model spectra were formed with regard to the features observed in the $P(QS)$ distribution and fit to the experimental spectra by varying the entire set of superfine parameters. The results of interpretation of the Mössbauer spectra are given in Table 1. The chemical shifts and quadrupole splittings for all the observed iron positions are characteristic of trivalent iron Fe^{3+} in the octahedral positions and are consistent with the literature data for Fe^{3+} in the iron hydroxides [53].

For samples 0 h, 3 h, and 8 h, the data obtained agree well with the results reported in [49]; iron atoms in bacterial ferrihydrite can occupy three positions with different quadrupole splittings. Iron positions Fe1 and Fe2 are designated as in studies [45,46] and correspond to the cubic and hexagonal ligand packing. These positions are crystal-chemical analogs of the spinel and hematite phases in the local environment of an iron cation. Their population weakly varies with time of the heat treatment. Position Fe3 corresponds to the interlayer iron atoms and its population for samples 24 h and 240 h is much smaller.

The long-term (24–240 h) heat treatment results in the two noticeable effects: new iron positions with the higher and lower local symmetries relative to the initial sample arise and the population of the interlayer positions decreases. This is indicative of both rearrangement and ordering of the structure of crystallographic formations.

Fig. 2 shows typical TEM micrographs of samples 0 h and 24 h. Coarsening of particles after heat treatment can be seen from these micrographs. Average size of ferrihydrite nanoparticles estimated from several micrographs found out to be ~ 2.7 nm and ~ 4 nm for samples 0 h and 24 h respectively. These values are in good agreement with that obtained below from the analysis magnetic data (Table 2).

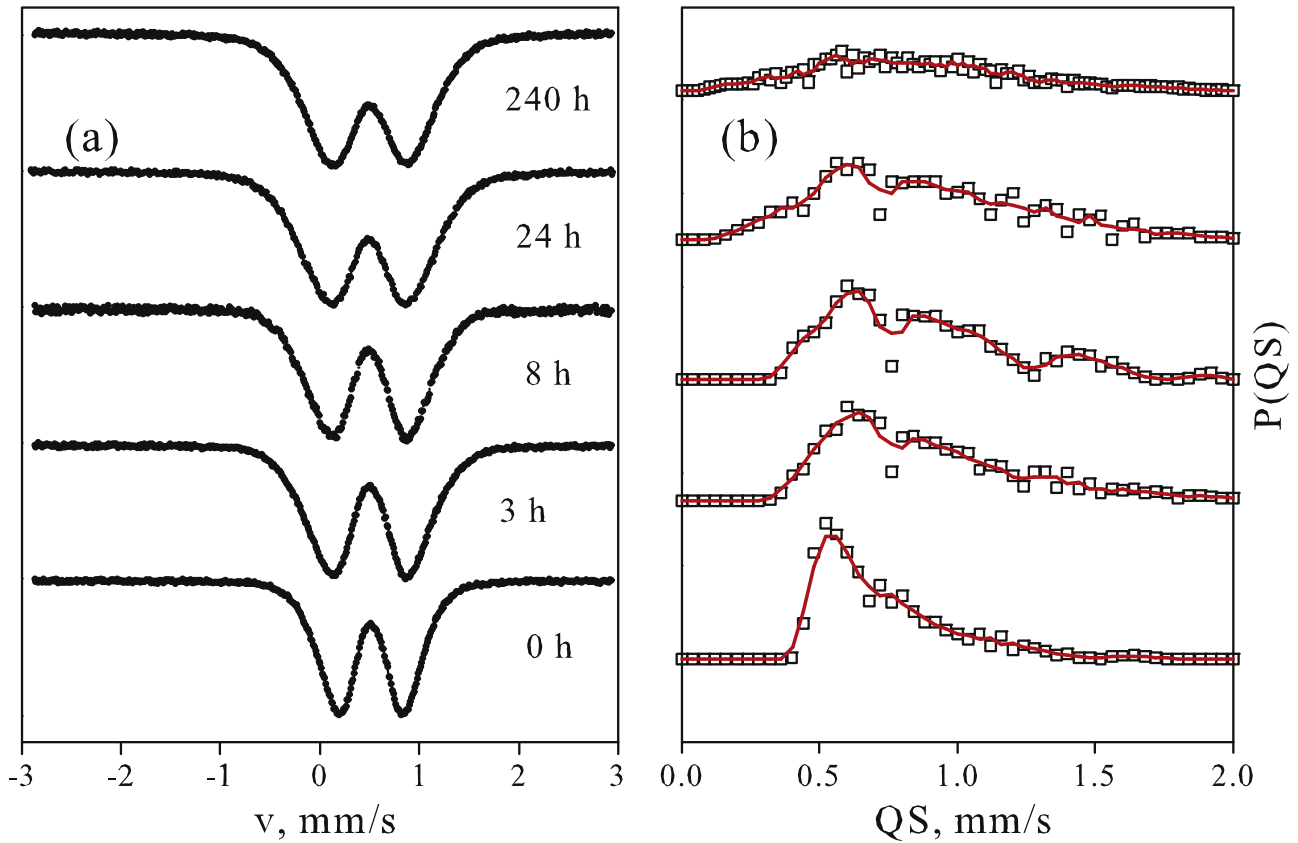


Fig. 1. (a) Room-temperature Mössbauer spectra and (b) distribution of quadrupole splittings $P(QS)$.

Table 1

Mössbauer parameters of bacterial ferrihydrite. IS – chemical shift, QS – quadrupole splitting, W – is the full width at half maximum of the absorption line, A-fractional site occupancy, Positions, designed as Fe1 and Fe2 correspond to cubic and hexagonal ligand arrangement, Fe3 corresponds to interlayer iron atoms.

sample (h)	IS (± 0.005 mm/sec)	QS (± 0.01 mm/sec)	W (± 0.01 mm/sec)	A (± 0.03)	Position
0	0.334	0.45	0.24	0.24	Fe1 – cubic
	0.334	0.69	0.28	0.41	Fe2 – hex.
	0.320	1.00	0.40	0.35	Fe3 – interlayer
3	0.323	0.55	0.28	0.28	Fe1
	0.318	0.86	0.34	0.43	Fe2
	0.314	1.29	0.47	0.29	Fe3
8	0.314	0.50	0.26	0.21	Fe1
	0.316	0.81	0.34	0.46	Fe2
	0.302	1.23	0.43	0.33	Fe3
24	0.323	0.33	0.28	0.11	
	0.335	0.63	0.33	0.37	Fe1
	0.332	0.95	0.31	0.28	Fe2
240	0.325	1.29	0.30	0.16	Fe3
	0.324	1.67	0.33	0.08	
	0.300	0.25	0.27	0.09	
240	0.328	0.55	0.32	0.32	Fe1
	0.328	0.84	0.29	0.28	Fe2
	0.328	1.12	0.27	0.16	Fe3
	0.324	1.40	0.27	0.09	
	0.319	1.74	0.31	0.06	

3.2. Temperature dependences of magnetization $M(T)$

Fig. 3a shows temperature dependences of magnetization measured in the field $H=1$ kOe under the ZFC and FC conditions. The $M(T)$ dependences are typical of an ensemble of SP particles: the $M(T)_{ZFC}$ and $M(T)_{FC}$ curves are different in the low-temperature region and the $M(T)_{ZFC}$ curves have maxima at characteristic temperature T_{max} , which significantly increases with annealing time. As is known, the shape of

the $M(T)$ curve and the T_{max} value depend on the size distribution of particles and, correspondingly, on their magnetic moment distribution [54–56]. However, at the log-normal size distribution, we may use average value $\langle T_B \rangle$, i.e., the maximum of the temperature dependence of $d(M(T)_{ZFC}-M(T)_{FC})/dT$ [55,56]. Fig. 3b shows temperature dependences of $d(M(T)_{ZFC}-M(T)_{FC})/dT$ for the investigated samples. It can be seen that $\langle T_B \rangle$ increases with annealing time, similar to T_{max} in Fig. 3b.

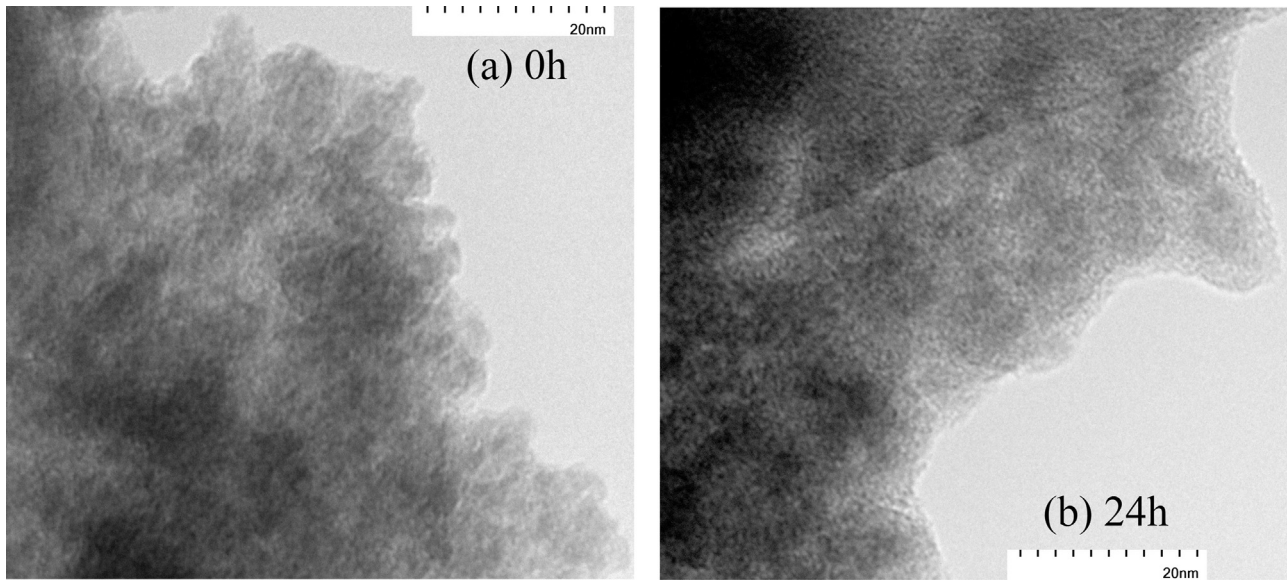


Fig. 2. TEM micrographs of samples 0 h and 24 h (for details see Section 2.1 and Section 3.1).

Table 2
Some parameters of studied samples, derived from experimental $M(T)$ dependences (T_{\max} – Fig. 3a, $\langle T_B \rangle$ – Fig. 3b) and fitting of the $M(H)$ dependences by expression (4) (s^2 – dispersion of log-normal function, N_p – the amount of particles per gram, the values $\langle \mu_p \rangle (T=0)$, $\chi_{AF}(T=0)$). The T_{Nex} values are obtained by extrapolation of data of Fig. 6, and the mean particle size $\langle D \rangle$ is obtained by expression (9) from $\langle \mu_p \rangle (T=0)$ and s^2 data).

(h)	T_{\max} , K	$\langle T_B \rangle$, K	s^2	$N_p (\times 10^{18})$	$\chi_{AF}(T=0)$, (10^{-4} emu/Oe g)	T_{Nex} , K	$\langle \mu_p \rangle (T=0)$, μ_B	$\langle D \rangle$, nm
0	26	12	0.2	2.5	0.64	360	162	3.1
3	48	20	0.3	1.6	0.47	420	230	3.8
8	72	35	0.36	1.8	0.56	500	251	4.1
24	78	39	0.49	2.2	0.57	540	302	4.5
240	85	40	0.64	2.1	0.6	540	315	4.6

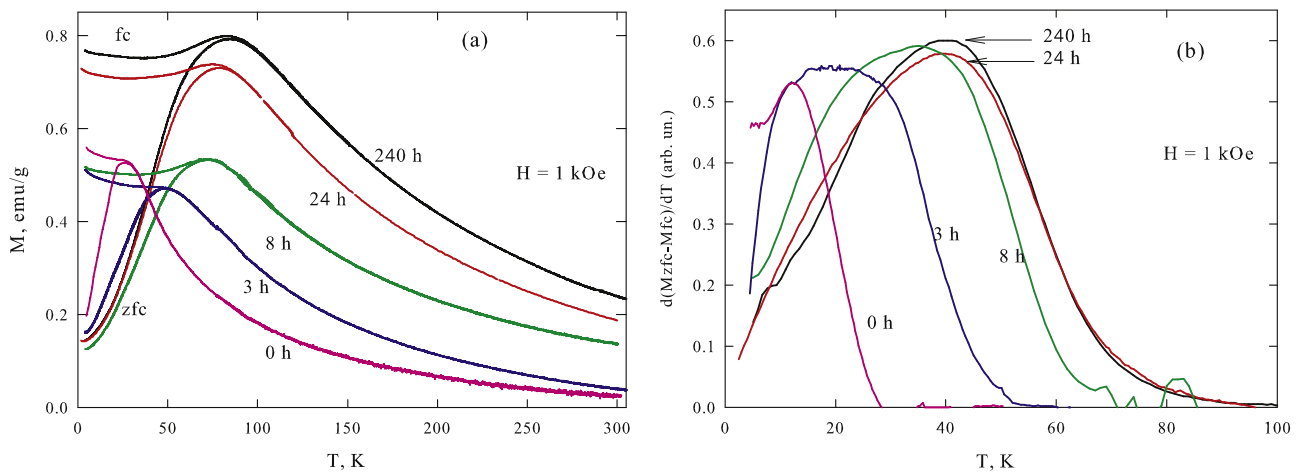


Fig. 3. Temperature dependences (a) of magnetic moment in the field $H=1$ kOe under the ZFC and FC conditions and (b) of derivative $d(M(T)_{ZFC}-M(T)_{FC})/dT$ for the investigated samples.

The T_{\max} values for the investigated samples significantly depend on an external field, as can be seen from the $M(T)_{ZFC}$ and $M(T)_{FC}$ curves obtained in the external fields $H=1.0, 5.0, 10,$ and 30 kOe (Figs. 4a–c show this behavior for samples 0 h, 8 h and 240 h respectively). The significant shift of temperature T_{\max} and the temperature of the irreversible behavior of the $M(T)$ dependence toward lower temperatures, as well as the change in the $M(T)$ dependences with increasing external field indicate that the investigated systems of ferrihydrite nanoparticles are superparamagnetic.

According to the generally accepted concepts, the blocking temperature is unambiguously related to particle volume V as

$$T_B = KV / \ln(\tau/\tau_0) k. \quad (2)$$

Here, K is the magnetic anisotropy constant and k is the Boltzmann constant. The ratio between the characteristic measuring time $\tau \sim 10^2$ s and characteristic particle relaxation time $\tau_0 \sim 10^{-9} - 10^{-10}$ s yields the factor $\ln(\tau/\tau_0) \approx 25$ in the denominator of Eq. (2). Assuming the anisotropy constant to be approximately invariable, we can attribute the growth of the T_{\max} and

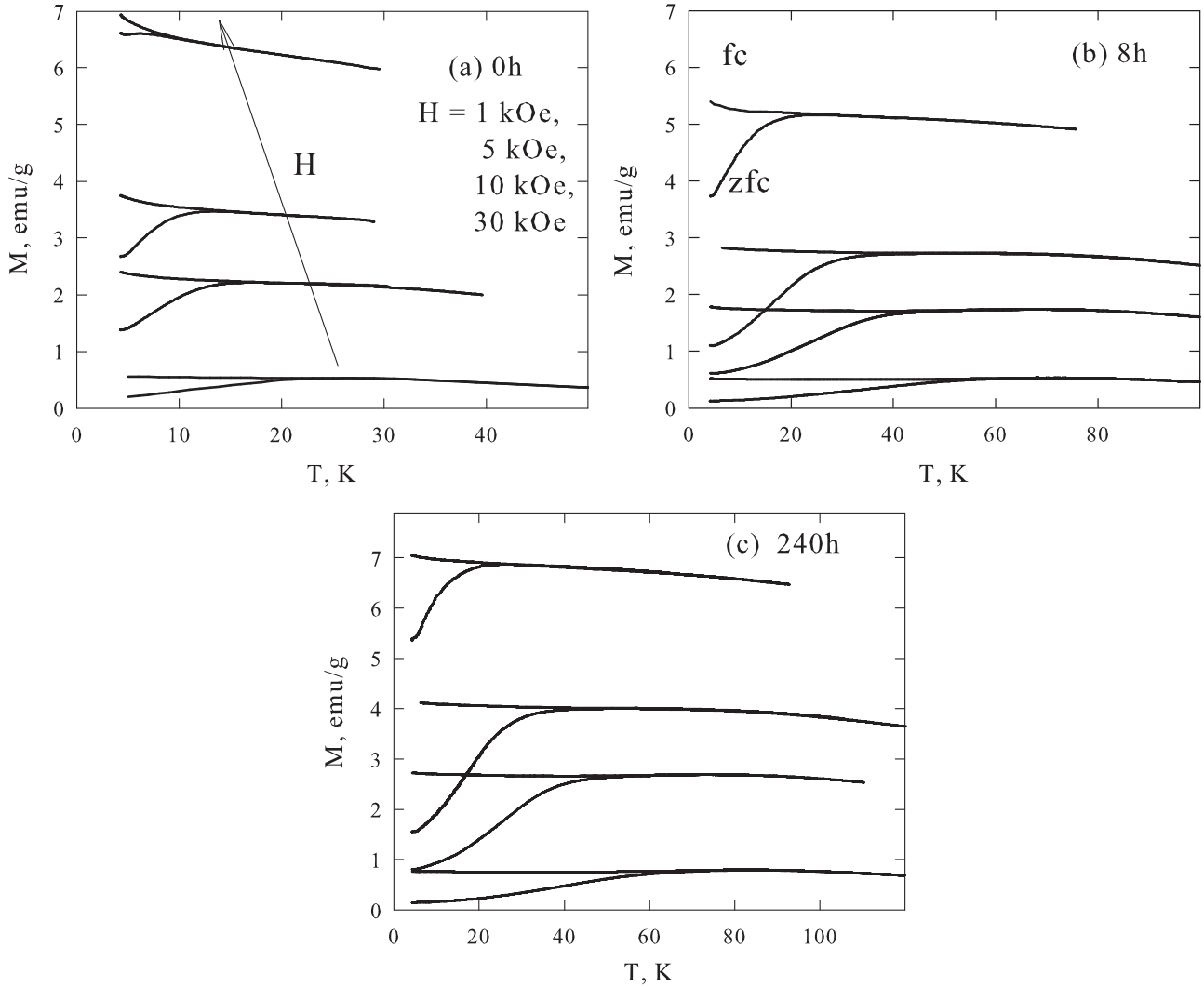


Fig. 4. Temperature dependences of magnetic moment in fields of 1–30 kOe under the ZFC and FC conditions for the samples 0 h (a), 8 h (b) and 240 h (c). The range along the X axis is different for (a–c).

$\langle T_B \rangle$ values to an increase in the particle volume during annealing. To check this assumption, we measured and analyzed the $M(H)$ curves at temperatures above T_{\max} .

3.3. Analysis of magnetization curves above the blocking temperature

It is usually assumed that the interparticle interaction does not play a key role in magnetization of small AF ordered particles [7]. For example, in ferritin it is the protein shell that leads to spatial separation of magnetically active phases of particles and minimizes the interparticle magnetic interactions. The particles investigated here are also coated with an organic shell, which covers the entire particle surface [46,47,51], since the particles are formed on the outer surface of bacteria. Therefore, in our analysis we ignore the interparticle interactions. The monotonic variation in T_{\max} during annealing additionally proves the validity of such an approach.

Typical experimental $M(H)$ dependences for the investigated samples in the temperature range $T > T_{\max}$ are presented in Fig. 5 (symbols). In the simplest case, above the blocking temperature the $M(H)$ dependence of a system of small noninteracting AF particles can be described by the expression (see, e.g., [7])

$$M(H) = M_S \times L(\mu_p, H) + \chi_{AF} \times H. \quad (3)$$

Here, M_S is the saturation magnetization of a system of SP particles, μ_p is the average magnetic moment of a particle, and $L(\mu_p, H)$ is the Langevin function:

$$L(\mu_p, H) = \coth(\mu_p \times H/kT) - 1/(\mu_p \times H/kT).$$

The term $\chi_{AF} \times H$ describes the AF particle sublattice cant (χ_{AF} is the magnetic susceptibility). However, at the real size distribution of particles, Eq. (3) describes the experimental data incompletely [37,38,42,54]. For the distribution function $f(\mu_p)$ of the magnetic moment of particles, the $M(H)$ dependence is described as

$$M(H) = N_p \int_0^\infty L(\mu_p, H) f(\mu_p) \mu_p d\mu_p + \chi_{AF} \times H. \quad (4)$$

Here, N_p is the number of particles in a powder unit mass and the integration is usually limited to the value $\mu > \mu_{\max}$, at which the $f(\mu_p)$ value becomes vanishingly small. To analyze the experimental data presented in Fig. 5, we used the log-normal distribution $f(\mu_p) = (\mu_p \cdot s \cdot (2\pi)^{1/2})^{-1} \exp\{-[\ln(\mu_p/n)]^2/2s^2\}$ with the average magnetic moment of a particle $\langle \mu_p \rangle = n \cdot \exp(s^2)$, where s^2 is the dispersion of value $\ln(\mu_p)$ [37,38,9].

Fitting of the experimental data by Eq. (4) uses four parameters. However, for each sample, number of particles N_p and dispersion s^2 of the distribution function were constant at different

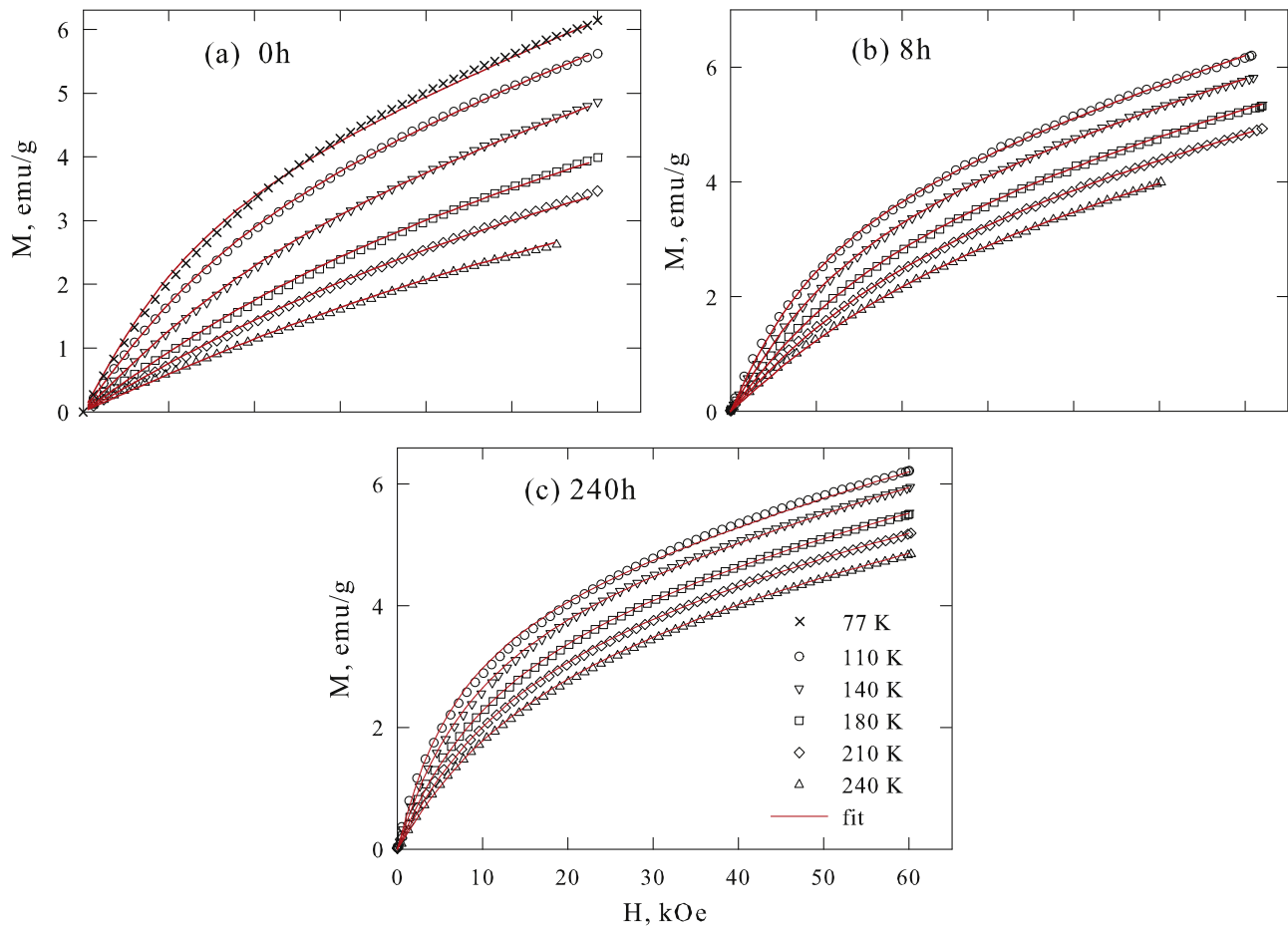


Fig. 5. Magnetization curves $M(H)$ at different temperatures $T > T_{\max}$ (symbols) for samples 0 h (a), 8 h (b) and 240 h (c). Solid curves indicate the data of the best fit by Eq. (4).

temperatures and the two varied parameters were average magnetic moment $\langle \mu_p \rangle$ of a particle (parameter n) and AF susceptibility χ_{AF} . To describe the experimental data by Eq. (4), we used the automatic step-by-step fitting of the $M(H)$ dependences under the condition of the minimum resulting difference between the experiment and fitting curves. The best fit results are shown in Fig. 5 by solid lines. Good agreement is reached in a wide temperature range, except for the region above T_{\max} by 20–30 K, which is apparently due to the anisotropy effect [7,36,44]. The s^2

and N_p values are given in Table 2.

3.4. Temperature dependences of $\langle \mu_p \rangle$ and χ_{AF}

Temperature dependences of the parameters $\langle \mu_p \rangle(T)$ and $\chi_{AF}(T)$, which were varied during the fitting are shown in Fig. 6. It can be seen that the average magnetic moment of a particle monotonically increases with annealing time (Fig. 6a). The pronounced dependence of χ_{AF} on annealing time is not observed

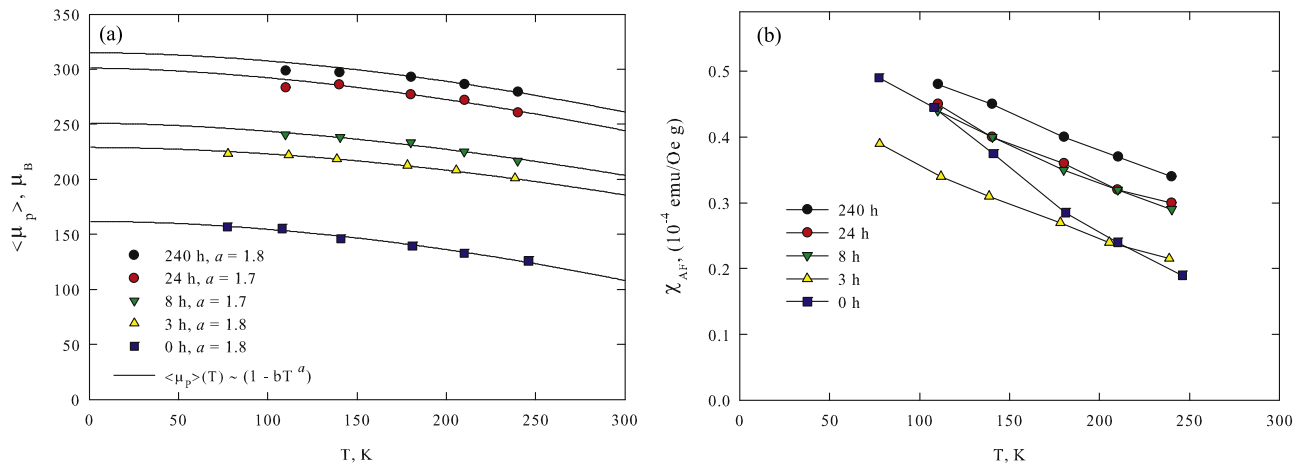


Fig. 6. Temperature dependences of (a) average magnetic moment $\langle \mu_p \rangle(T)$ of a particle and (b) AF susceptibility $\chi_{AF}(T)$ obtained from the conditions of the best agreement between the experimental and fitting $M(T)$ dependences (Fig. 5). Solid curves in Fig. 6a indicate the fitting of the obtained data by dependence (6). The values of exponent a are shown in the figure. Lines in Fig. 6b are eye guides, although the approximately linear $\chi_{AF}(T)$ dependence is discussed in the text.

(Fig. 6b), although there is the approximately linear temperature dependence of χ_{AF} :

$$\chi_{AF}(T) \approx \chi_{AF}(T=0) \times (1 - T/T_{Nex}). \quad (5)$$

Here, T_{Nex} is the temperature at which extrapolation of the data to the high-temperature region yields $\chi_{AF}=0$. Dependence (5) was observed for ferrihydrite [26–28] and ferritin [27,38,40] nanoparticles; the T_{Nex} value was unambiguously related to the Néel point of an antiferromagnet. The T_{Nex} values in Fig. 6b, which were obtained by extrapolation of the data to $\chi_{AF}=0$, are given in Table 2. If this value for the initial sample is close to the Néel temperature of ferrihydrite [26–28,38,40], then we may state the T_{Nex} growth with annealing time. As follows from the Mössbauer spectroscopy data, the long-time annealing leads not only to the occurrence of new iron positions, but also to the ordering of the structure of local formations, which can enhance the magnetic ordering temperature.

Now, let us consider the behavior of the $\langle \mu_p \rangle (T)$ dependence (Fig. 6a) for the investigated samples. The experimental $\langle \mu_p \rangle (T)$ data, except for the temperature region near T_{max} , agree satisfactorily with the dependence

$$\langle \mu_p \rangle (T) \sim \langle \mu_p \rangle (T=0) \times (1 - CT)^a. \quad (6)$$

This dependence was observed for ferri- and ferromagnetic nanoparticles [19,57–60]. Exponent a was often different from the value of $3/2$, which follows from the classical consideration of spin waves in bulk ferri- and ferromagnets (the Bloch's law) [19,60]. For NiO [9], ferritin, and ferrihydrite AF nanoparticles [26,28,34,35], the $\langle \mu_p \rangle (T)$ dependence is often more complex and sometimes the $\langle \mu_p \rangle$ value increases with temperature. The thermoinduced contribution to the magnetic moment of an AF particle was considered to be a possible reason for such a behavior [41]. However, as was demonstrated in [38], if the distribution function of the magnetic moment is taken into account, then the $\langle \mu_p \rangle (T)$ dependence monotonically decreases, in contrast to the increasing dependence obtained with disregard of the distribution function. In studies [37,38], the value $a \approx 2$ for ferritin particles was obtained. The a values for the samples investigated here lie within 1.7–1.8 (Fig. 6a). It should be noted that as the annealing time is increased, the $\langle \mu_p \rangle (T)$ dependences indicate the variation in coefficient C , which decreases in Eq. (6). As a result, the value of exponent a for samples annealed for longer times is determined with lower accuracy. Extrapolation of dependence (6) to the high-temperature region, where $\langle \mu_p \rangle = 0$, yields values of about 550 and 750 K for samples 0 h and 3 h and about 800 K for the rest samples. This is consistent with an increase in T_{Nex} (Fig. 6a) upon long-time annealing. Note that extrapolation of the $\langle \mu_p \rangle (T)$ dependences yields, as a rule, overestimated values of the magnetic ordering temperature. This can be explained by different temperature regions of validity of (Eqs. (5) and 6): Eq. (6) describes the experimental results only in the low-temperature region, since even at the ferri- or ferromagnetic ordering the Bloch's law (Eq. (6) at $a=3/2$) is valid only in the low-temperature region.

3.5. Blocking temperature as a function of particle volume: Evidence of the surface effect

The unambiguous conclusion drawn from the fitting of the $M(H)$ dependences is the growth of the average magnetic moment of a particle upon annealing. Taking into account relations (1) and (2) and the blocking temperature growth (Fig. 3 and Table 2), we may conclude that upon annealing the particles coarsen (in accordance with results of TEM, Fig. 2), which is accompanied by the mass loss (18–26%, see Section 2.1.). Since the annealing temperature is low (160 °C), a decrease in the mass of a sample

prepared by drying the water sol is most likely due to the partial loss of water and organic shell of particles. Upon sublimation of the organic shell of close nanoparticles, the latter agglomerate and the average particle size increases. As a result, the fraction of coarse particles grows, which leads to an increase in parameter s^2 of the log-normal distribution (Table 2).

We will estimate the particle size from Eq. (1) with the use of the values of magnetic moment $\mu_p(T=0)$ from Table 2, which were determined by extrapolation of the $\mu_p(T)$ data in the low-temperature region with sufficient accuracy (Fig. 6a). In most studies on the magnetic properties of ferritin and ferrihydrite nanoparticles [7,26,28,34–38], the exponent in Eq. (1) was found to be close to $1/2$. Our previous investigations of bacterial ferrihydrite taken from the other set, together with the results of microstructure investigations [47], also confirmed the validity of Eq. (1) at $n \approx 1/2$ for the initial sample annealed under the same conditions for 3 h [49,50]. In view of the aforesaid, we have the magnetic moment $\mu_p \sim N_{Fe}^{1/2}$ and the number of iron atoms in a particle $N_{Fe} \sim (\mu_p)^2$. Assuming that Fe^{3+} has only the spin moment ($\mu_{Fe^{3+}} \approx 5\mu_B$, where μ_B is the Bohr magneton), we obtain $N_{Fe} \approx (\mu_p/5)^2$, where the magnetic moment of a particle is determined in Bohr magnetons. Hence, the linear particle size is obviously expressed as

$$D \approx d_{Fe-Fe} \times N_{Fe}^{1/3} \approx d_{Fe-Fe} \times (\mu_p/5)^{2/3}, \quad (7)$$

where d_{Fe-Fe} is the mean distance between Fe atoms. Thus, we arrive at the expression for the particle volume:

$$V \approx D^3 \approx (d_{Fe-Fe})^3 \times (\mu_p/5)^2. \quad (8)$$

The used parameters of the log-normal distribution $f(\mu_p)$ (Table 2) show that the magnetic moment distribution of particles is sufficiently broad and, since dependence (8) is quadratic, the volume distribution of particles is broad as well. Therefore, it is reasonable to use average values $\langle D \rangle$ and $\langle V \rangle$. Then, instead of (Eqs. (7) and 8), we obtain

$$\langle D \rangle = d_{Fe-Fe} \int_0^\infty f(\mu_p) (\mu_p/5)^{2/3} d\mu_p, \quad (9)$$

$$\langle V \rangle = (d_{Fe-Fe})^3 \int_0^\infty f(\mu_p) (\mu_p/5)^2 d\mu_p. \quad (10)$$

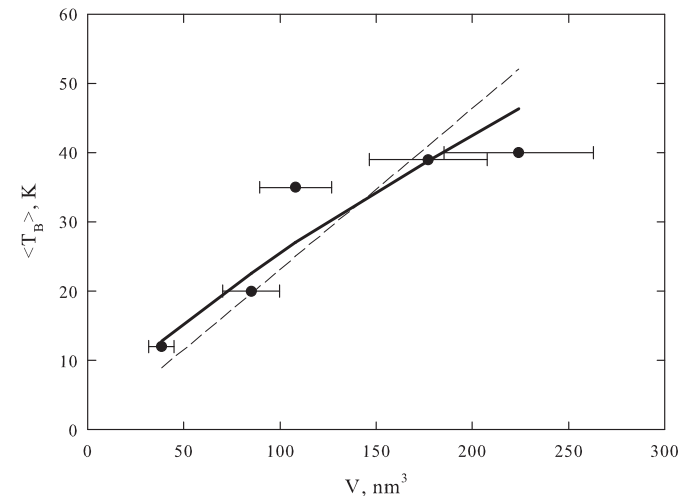


Fig. 7. Dependence of average blocking temperature $\langle T_B \rangle$ (Fig. 3b) of the investigated samples on average particle volume $\langle V \rangle$ (symbols) obtained using Eq. (10) with the parameters of the distribution function $f(\mu_p)$ for the best fit of the $M(H)$ dependences (Fig. 5 and Table 2). The dashed straight indicates the approximation of experimental data by Eq. (2) at $K \approx 8 \times 10^5$ erg/cm³. The solid curve indicates the approximation by Eqs. (11) and (12) at $K_V \approx 1.7 \times 10^5$ erg/cm³ and $K_S \approx 0.055$ erg/cm².

To determine $\langle D \rangle$ and $\langle V \rangle$, we use the parameters of log-normal distribution $f(\mu_p) \sim s^{-2}$ and $\langle \mu_p \rangle$ obtained during fitting of the $M(H)$ dependences (Fig. 4). The $d_{\text{Fe-Fe}}$ value was taken equal to 0.31 nm [28]. The $\langle D \rangle$ values obtained from Eq. (9) are given in Table 2. A noticeable increase in $\langle D \rangle$ reflects coarsening of particles with an increase in annealing time, which is related to an increase in the blocking temperature (see Figs. 2 and 3 and Table 2) in accordance with Eq. (2).

In the further analysis, we assume the $\langle T_B \rangle$ values to be consistent with the average particle volume (Fig. 3b) and, to explain the functional dependence $\langle T_B \rangle$ on V from the experimental data, we use the $\langle V \rangle$ values determined from Eq. (10) (note that for a sufficiently broad distribution, we have $\langle V \rangle \neq \langle D \rangle^3$). The dependence of $\langle T_B \rangle$ on $\langle V \rangle$ is shown in Fig. 7. It can be seen that experimental points are not described by the linear dependence predicted by Eq. (2). The obtained dependence of $\langle T_B \rangle$ on $\langle V \rangle$ is characterized by the negative curvature sign. Such a behavior is consistent with the concept about the presence of an additional contribution to the magnetic anisotropy, specifically, the surface anisotropy characteristic of small particles. In the simplest way, the surface anisotropy contribution to effective anisotropy K_{eff} of a particle with linear size D can be taken into account as [61]

$$K_{\text{eff}} = K_V + \frac{6K_S}{D}, \quad (11)$$

where K_V and K_S are the bulk and surface anisotropy constants, respectively. Then, we rewrite dependence (2) in the form

$$T_B \approx K_{\text{eff}} V / 25 k. \quad (12)$$

Fig. 7 shows the results of processing of experimental points by dependence (2) with regard to only the bulk anisotropy (linear dependence, Eq. (2)) and to both the bulk and surface anisotropies with the use of Eqs. (11) and (12). It can be seen that, in the latter case, the experimental points are better described. Satisfactorily agreement with the experiment is reached at the values $K_V \approx 1.7 \times 10^5 \text{ erg/cm}^3$ ($\pm 0.5 \times 10^5 \text{ erg/cm}^3$) and $K_S \approx 0.055 \text{ erg/cm}^2$ ($\pm 0.005 \text{ erg/cm}^2$). The obtained bulk magnetic anisotropy constant is consistent with the value $K \approx 1 \times 10^5 \text{ erg/cm}^3$ reported in study [31], where this constant was determined for synthesized ferrihydrite particles from the frequency dependences of the blocking temperature. In studies [30,36,62], the effective magnetic anisotropy of ferritin and ferrihydrite particles determined using different techniques lie within

$(2.5 \div 6) \times 10^5 \text{ erg/cm}^3$. The value $K \approx 8 \times 10^5 \text{ erg/cm}^3$ ($\pm 5\%$) obtained with disregard of the surface anisotropy (linear dependence in Fig. 7) is similar to the K_{eff} value for the smallest particles (sample 0 h) and is obviously overestimated to be used as the bulk anisotropy constant of ferrihydrite.

3.6. Hysteresis dependences of magnetization

Fig. 8 shows typical hysteresis dependences $M(H)$ at $T=4.2 \text{ K}$ for the samples under study. The value of coercivity H_C increases with annealing time (see the insert of Fig. 8¹). Although hysteresis loops presented in Fig. 8 are open ones, up to the used maximum field H_{max} of 60 kOe, it is reasonable to assume that increase of $H_C(H_{\text{max}}=60 \text{ kOe})$ is related to the similar behavior of coercivity of closed hysteresis. On the author's opinion observed enhance of H_C ($T=4.2 \text{ K}$, $H_{\text{max}}=60 \text{ kOe}$) with annealing time corresponds to the increase of particles in size during the heat treatment in spite of the fact that hysteresis loops are opened. To estimate the coercivity, we use the well-known relation, which follows from the Stoner–Wohlfarth model for noninteracting single-domain particles [63]

$$H_C \approx \frac{K}{M_S} \left[1 - (T/T_B)^{1/2} \right], \quad (13)$$

where M_S is the saturation magnetization of a particle. Let us estimate H_C for particles with average volume. According to Eq. (8), the magnetic moment of a particle is determined as $\mu_p \approx \langle V \rangle / (d_{\text{Fe-Fe}})^{3/2} \times 5\mu_B$. Since $M_S = \mu_p / V$, the M_S value is estimated as $M_S \approx d_{\text{Fe-Fe}}^{-3/2} V^{-1/2} \times 5\mu_B$. Substituting the M_S values determined in such a way and corresponding blocking temperatures $\langle T_B \rangle$ in Eq. (13) and using effective magnetic anisotropy constant K_{eff} (Eq. (11)) at the above-mentioned K_V and K_S values, we obtain $H_C(4.2 \text{ K})$ of about 10, 16, 21, 24, and 26 kOe for samples 0 h, 3 h, 8 h, 24 h, and 240 h, respectively. These estimates exceed the experimental $H_C(T=4.2 \text{ K}, H_{\text{max}}=60 \text{ kOe})$ values (see insert to Fig. 8) and there are two factors responsible for larger values of estimated coercivity. As it was mentioned above, the $M(H)$ hysteresis loops presented in Fig. 8 are open ones, and therefore, the experimental $H_C(T=4.2 \text{ K}, H_{\text{max}}=60 \text{ kOe})$ values are less than coercivity of the limit hysteresis loop. Secondly, particles are distributed by size, volume, and, consequently, by M_S and T_B values, which affect the resulting H_C value [64]. Nevertheless, the estimates obtained are in qualitative agreement with observed enhance of H_C with annealing time which additionally reveals increase of particles in size during the heat treatment.

Note another feature of the hysteresis $M(H)$ dependences in Fig. 8. In a certain magnetic field range, the initial magnetization curve is located beyond the hysteresis curve. After cancellation of the thermomagnetic prehistory of a sample, i.e., its heating above T_{max} and cooling under the ZFC conditions, the effect is repeated. Such a behavior was observed by us on the bacterial ferrihydrite samples from the other set [50]. In addition, the observation of such an anomalous hysteresis was reported for some SP particles [65,66]. This nontrivial effect, along with the detected shift of the hysteresis loop [50] under the FC conditions from the temperature above T_{max} , can be attributed to complex structure of energy barriers induced by the magnetic anisotropy [32]. The above-mentioned effects will be analyzed in the nearest future.

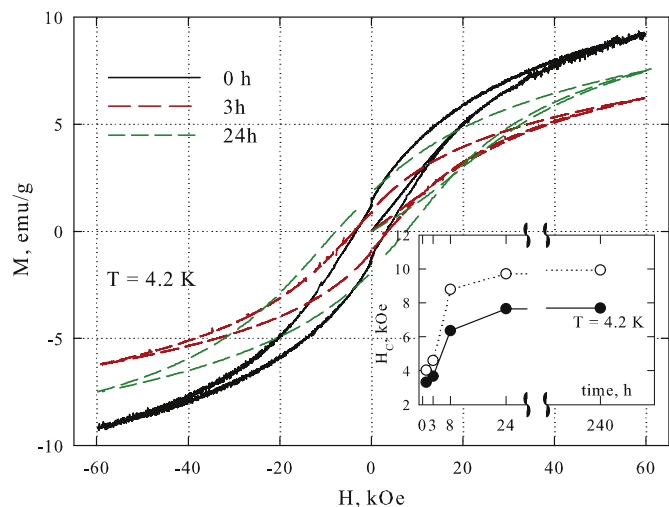


Fig. 8. Hysteresis dependences $M(H)$ for the investigated samples at temperature $T=4.2 \text{ K}$ and the maximum applied field $H_{\text{max}}=60 \text{ kOe}$. Insert: dependence of coercivity H_C at $H_{\text{max}}=60 \text{ kOe}$ on annealing time (closed symbols) and the same dependence obtained by subtracting the AF component $\chi_{\text{AF}} \times H$ (open symbols).

¹ The experimental $M(H)$ curves contain the χ_{AF} contribution linear with respect to the field (term $\chi_{\text{AF}} \times H$ in Eqs. (3) and (4)), which remains at temperatures below the blocking temperature. The account for this contribution somewhat corrects the $H_C(4.2 \text{ K})$ data for the samples under study, which can be seen in the insert to Fig. 8 (open symbols).

4. Conclusions

We studied modification of the magnetic properties of the system of bacterial ferrihydrite nanoparticles subjected to the heat treatment at temperatures somewhat higher than the boiling point of water. The initial crystal-chemical structure of ferrihydrite is disordered due to the nanometer size of comprising particles. The heat treatment at $T=160^{\circ}\text{C}$ for times of up to 240 h induces additional defects in the ferrihydrite structure, but, according to the Mössbauer spectroscopy data, does not lead to the formation of any other iron oxide or hydroxide phases. The antiferromagnetic ordering of iron atoms in ferrihydrite together with its defect structure result in the occurrence of the uncompensated magnetic moment in nanoparticles and, consequently, in the superparamagnetic behavior of the spin system with characteristic blocking temperatures. The data obtained in this work and previous studies allow us to conclude that uncompensated magnetic moment μ_{un} is caused by defects on the surface of a particle and in its bulk, which is consistent with the Néel hypothesis about proportionality of the μ_{un} value to the number of defects raised to the power of 1/2.

The standard analysis of the magnetization curves for the investigated samples with the use of the distribution functions of the magnetic moment of particles with regard to the AF contribution showed that the average magnetic moment of particles and blocking temperature T_B monotonically increase with annealing time. Thus, we concluded that particles of the initial powder coarsen upon heat treatment. This is confirmed also by the particle mass loss (intercrystallite water and organic sediments) because of partial burning of the organic shell, which leads to agglomeration of particles. The temperature evolution of the uncompensated magnetic moment follows the dependence similar to the well-known Bloch's law ($\sim 1-T^a$), which is caused by the excitation of spin waves in bulk ferri- and ferromagnets, although exponent a differs from the classical value of 3/2 and amounts to 1.7–1.8.

Based on the above-mentioned Néel hypothesis and the data obtained from the distribution function of the magnetic moment of particles and blocking temperatures, we established that the processes of blocking of ferrihydrite nanoparticles are affected by both the bulk and surface anisotropies. The corresponding bulk and surface anisotropy constants were determined. The contribution of the surface anisotropy apparently plays a key role in the behavior of magnetization hysteresis below the blocking temperature: the investigated samples exhibit the coercivity $H_C \sim 4\text{--}8\text{ kOe}$ at a temperature of 4.2 K, although the hysteresis loops are minor in the maximum external fields of up to 90 kOe.

The growth of the particle size upon low-temperature heat treatment of the samples established by analyzing their magnetic properties is of great practical importance. We have found a simple way of controlling (increasing) the particle size. According to our data, exposure of the powder of annealed nanoparticles in air at room temperature and humidity of 100% for a long time (tens of hours) or water impregnation and drying at room temperature under the standard conditions do not change the magnetic properties, including the blocking temperature and shape of magnetization curves. Hence, the low-temperature heat treatment enhances the magnetic moment of particles. At room temperature, they are in the superparamagnetic state, but their size and magnetic properties remain stable in an aqueous medium. The latter can play a decisive role for application of the investigated material as a drug carrier in the human body.

Acknowledgments

TEM studies were performed on facility of Resource Sharing Center of Krasnoyarsk Scientific Center of Siberian Branch of

Russian Academy of Sciences. Authors acknowledge to M.N. Volochaev for the TEM measurements.

References

- [1] N. Amin, S. Arajs, *Phys. Rev. B* 35 (N10) (1987) 4810.
- [2] J.T. Richardson, D.I. Yiagas, B. Turk, K. Forster, M.V. Twigg, *J. Appl. Phys.* 70 (1991) 6977.
- [3] S.A. Makhlof, F.T. Parker, F.E. Spada, A.E. Berkowitz, *J. Appl. Phys.* 81 (8) (1997) 5561.
- [4] I.V. Golosovsky, I. Mirebeau, G. Andre, D.A. Kurdyukov, Yu.A. Kumzerov, S. B. Vakhrushev, *Phys. Rev. Lett.* 86 (2001) 5783.
- [5] J.L. Dormann, D. Fiorani, E. Tronc, *Adv. Chem. Phys.* 98 (1997) 283.
- [6] A. Punnoose, H. Magnone, M.S. Seehra, J. Bonevich, *Phys. Rev. B* 64 (2001) 174420.
- [7] S. Mørup, D.E. Madsen, C. Frandsen, C.R.H. Bahl, M.F. Hansen, *J. Phys. Condens. Matter* 19 (2007) 213202.
- [8] F. Bødker, M.F. Hansen, C.B. Koch, K. Lefmann, S. Mørup, *Phys. Rev. B* 61 (10) (2000) 6826.
- [9] I.V. Tiwari, K.P. Rajeev, *Solid State Commun.* 152 (2012) 1080.
- [10] R.D. Zysler, D. Fiorani, A.M. Testa, L. Suber, E. Agostinelli, M. Godinho, *Phys. Rev. B* 68 (2003) 212408.
- [11] S. Mukherjee, A.K. Pal, S. Bhattacharya, S. Chattopadhyay, *J. Phys.: Condens. Matter* 20 (2008) 055204.
- [12] J. Wang, W. Wu, F. Zhao, G. Zhao, *J. Appl. Phys.* 109 (2011) 056101.
- [13] X.G. Zheng, C.N. Xu, K. Nishikubo, K. Nishiyama, W. Higemoto, W.J. Moon, E. Tanaka, E.S. Otake, *Phys. Rev. B* 72 (2005) 014464.
- [14] A.E. Bianchi, I.2 S.J. Stewart, I. R.D. Zysler, G. Punte, *J. Appl. Phys.* 112 (2012) 083904.
- [15] Yu.A. Kumzerov, N.F. Kartenko, L.S. Parfen'eva, I.A. Smirnov, A.A. Sysoeva, H. Misiorek, A. Jezowski, *Phys. Solid State* 54 (5) (2012) 1066–1069.
- [16] N.J.O. Silva, M. Karmaoui, V.S. Amaral, I. Puente-Orench, J. Campo, I. da Silva, A. Ibarra, R. Bustamante, A. Millán, F. Palacio, *Phys. Rev. B* 87 (2013) 224429.
- [17] L. Néel, *C.R. Acad. Sci. Paris* 252 (1961) 4075.
- [18] Yu.L. Raikher, V.I. Stepanov, *J. Phys.: Condens. Matter* 20 (2008) 204120.
- [19] J.P. Chen, C.M. Sorensen, K.J. Klabunde, G.C. Hadjipanayis, E. Devlin, A. Kostikas, *Phys. Rev. B* 54 (1996) 9288.
- [20] P. Dutta, S. Pal, M.S. Seehra, N. Shah, G.P. Huffman, *J. Appl. Phys.* 105 (2009) 07B501.
- [21] S. Ayyappan, G. Panneerselvam, M.P. Antony, N.V. Rama Rao, N. Thirumurugan, A. Bharathi, J. Philip, *J. Appl. Phys.* 109 (2011) 084303.
- [22] V.L. Kirillov, D.A. Balaev, S.V. Semenov, K.A. Shaikhutdinov, O.N. Martyanov, *Mater. Chem. Phys.* 145 (2014) 75.
- [23] Q.A. Pankhurst, N.T.K. Thanh, S.K. Jones, J. Dobson, *J. Phys. D: Appl. Phys.* 42 (2009) 224001.
- [24] Q.A. Pankhurst, J. Connolly, S.K. Jones, J. Dobson, *J. Phys. D: Appl. Phys.* 36 (2003) R167.
- [25] K. Dobretsov, S. Stolyar, A. Lopatin, *Acta Otorhinolaryngol. Ital.* 35 (2) (2015) 97–102.
- [26] M.S. Seehra, V.S. Babu, A. Manivannan, J.W. Lynn, *Phys. Rev. B* 61 (2000) 3513.
- [27] M.S. Seehra, A. Punnoose, *Phys. Rev. B* 64 (2001) 1132410.
- [28] A. Punnoose, T. Phanthavady, M.S. Seehra, N. Shah, G.P. Huffman, *Phys. Rev. B* 69 (2004) 054425.
- [29] M.S. Seehra, V. Singh, X. Song, S. Bali, E.M. Eyring, *J. Phys. Chem. Solids* 71 (2010) 1362.
- [30] E.L. Duarte, R. Itri, E. Lima Jr, M.S. Baptista, T.S. Berquó, G.F. Goya, *Nanotechnology* 17 (2006) 5549.
- [31] T.S. Berquó, J.J. Erbs, A. Lindquist, R.L. Penn, S.K. Banerjee, *J. Phys.: Condens. Matter* 21 (2009) 176005.
- [32] N.J.O. Silva, V.S. Amaral, A. Urtizberea, R. Bustamante, A. Millan, F. Palacio, E. Kampert, U. Zeitler, S. de Brion, O. Iglesias, A. Labarta, *Phys. Rev. B* 84 (2011) 104427.
- [33] S. Gider, D.D. Awschalom, T. Douglas, K. Wong, S. Mann, G. Cain, *J. Appl. Phys.* 79 (8) (1996) 5324.
- [34] S.A. Makhlof, F.T. Parker, A.E. Berkowitz, *Phys. Rev. B* 55 (1997) R14717.
- [35] J.G.E. Harris, J.E. Grimaldi, D.D. Awschalom, A. Chilero, D. Loss, *Phys. Rev. B* 60 (1999) 3513.
- [36] C. Gilles, P. Bonville, K.K.W. Wong, S. Mann, *Eur. Phys. J. B* 17 (2000) 417.
- [37] C. Gilles, P. Bonville, H. Rakoto, J.M. Broto, K.K.W. Wong, S. Mann, *J. Magn. Magn. Mater.* 241 (2002) 430.
- [38] N.J.O. Silva, V.S. Amaral, L.D. Carlos, *Phys. Rev. B* 71 (2005) 184408.
- [39] R.P. Guertin, N. Harrison, Z.X. Zhou, S. McCall, F. Drymiotis, *J. Magn. Magn. Mater.* 308 (2007) 97.
- [40] N.J.O. Silva, A. Millan, F. Palacio, E. Kampert, U. Zeitler, V.S. Amaral, *Phys. Rev. B* 79 (2009) 104405.
- [41] S. Mørup, C. Frandsen, *Phys. Rev. Lett.* 92 (21) (2004) 217201.
- [42] N.J.O. Silva, L.D. Carlos, V.S. Amaral, *Phys. Rev. Lett.* 94 (2005) 039707.
- [43] S. Mørup, C. Frandsen, *Phys. Rev. Lett.* 94 (2005) 039708.
- [44] D.E. Madsen, S. Mørup, M.F. Hansen, *J. Magn. Magn. Mater.* 305 (2006) 95–99.
- [45] S.V. Stolyar, O.A. Bayukov, Yu.L. Gurevich, E.A. Denisova, R.S. Iskhakov, V. P. Ladygina, A.P. Puzyr, P.P. Pustoshilov, M.A. Bitekhtina, *Inorg. Mater.* 42 (7) (2006) 763.
- [46] S.V. Stolyar, O.A. Bayukov, Yu.L. Gurevich, V.P. Ladygina, R.S. Iskhakov, P.

- P. Pustoshilov, *Inorg. Mater.* 43 (6) (2007) 638.
- [47] M. Balasoiu, S.V. Stolyar, R.S. Iskhakov, L.A. Ischenko, Y.L. Raikher, A.I. Kuklin, O.L. Orelovich, Yu.S. Kovalev, T.S. Kurkin, *Rom. J. Phys.* 55 (7–8) (2010) 782.
- [48] Yu.L. Raikher, V.I. Stepanov, S.V. Stolyar, V.P. Ladygina, D.A. Balaev, L.A. Ishchenko, M. Balasoiu, *Phys. Solid State* 52 (2) (2010) 298.
- [49] D.A. Balaev, A.A. Dubrovskii, A.A. Krasikov, S.V. Stolyar, R.S. Iskhakov, V.P. Ladygina, E.D. Khilazheva, *JETP Lett.* 98 (3) (2013) 135.
- [50] D.A. Balaev, A.A. Krasikov, A.A. Dubrovskii, S.V. Semenov, O.A. Bayukov, S.V. Stolyar, R.S. Iskhakov, V.P. Ladygina, L.A. Ishchenko, *JETP* 119 (3) (2014) 479.
- [51] S.V. Stolyar, O.A. Bayukov, V.P. Ladygina, R.S. Iskhakov, L.A. Ishchenko, V. Yu Yakovchuk, K.G. Dobretsov, A.I. Pozdnyakov, O.E. Piksina, *Phys. Solid State* 53 (1) (2011) 100.
- [52] A.D. Balaev, Yu.V. Boyarshinov, M.M. Karpenko, B.P. Khrustalev, *Prib. Tekh. Eksp.* 3 (1985) 167.
- [53] *Mössbauer Mineral Handbook*, edited by J.G. Stevens, Mössbauer Effect Data Center, 2002.
- [54] M. El-Hilo, *J. Appl. Phys.* 112 (2012) 103915.
- [55] D. Tobia, E. Winkler, R.D. Zysler, M. Granada, H.E. Troiani, D. Fiorani, *J. Appl. Phys.* 106 (2009) 103920.
- [56] J.C. Denardin, A.L. Brandl, M. Knobel, P. Panissod, A.B. Pakhomov, H. Liu, X. Zhang, *Phys. Rev. B* 65 (2002) 064422.
- [57] J.F. Hochepeid, M.P. Pileni, *J. Appl. Phys.* 87 (5) (2000) 2472.
- [58] G.F. Goya, T.S. Berquo, F.C. Fonseca, M.P. Morales, *J. Appl. Phys.* 94 (5) (2003) 3520.
- [59] D.A. Balaev, A.A. Dubrovskiy, K.A. Shaykhtudinov, O.A. Bayukov, S. S. Yakushkin, G.A. Bukhtiyarova, O.N. Martyanov, *J. Appl. Phys.* 114 (2013) 163911.
- [60] C. Martínez-Boubeta, K. Simeonidis, M. Angelakeris, N. Pazos-Pérez, M. Giersig, A. Delimitis, L. Nalbandian, V. Alexandrakis, D. Niarchos, *Phys. Rev. B* 74 (2006) 054430.
- [61] F. Bødker, S. Mørup, S. Linderoth, *Phys. Rev. Lett.* 72 (1994) 282.
- [62] F. Luis, E. del Barco, J.M. Hernández, E. Remiro, J. Bartolomé, J. Tejada, *Phys. Rev. B* 59 (1999) 11837.
- [63] E.C. Stoner, E.P. Wohlfarth, *Philos. Trans. Roy. Soc. Lond. Ser. A* 240 (1948) 599.
- [64] S.V. Komogortsev, R.S. Iskhakov, A.D. Balaev, A.V. Okotrub, A.G. Kudashov, N. A. Momot, S.I. Smirnov, *Phys. Solid State* 51 (11) (2009) 2286.
- [65] P. Zhang, F. Zuo, F.K. Urban, A. Khabari, P. Griffiths, A. Hosseini-Tehrani, *J. Magn. Magn. Mater.* 225 (2001) 337.
- [66] E. Lima Jr., J.M. Vargas, H.R. Rechenberg, R.D. Zysler, *J. Nanosci. Nanotechnol.* 8 (2008) 5913.